

Numerical Simulations of Flow Bifurcations Inside a Driven Cavity

E.M. Wahba^C

*Mechanical Engineering Department, American University of Sharjah,
P.O. Box 26666 Sharjah, United Arab Emirates*

Received: 05/04/2011 – Revised 12/06/2011 – Accepted 16/06/2011

Abstract

Time-dependent numerical simulations for incompressible flow in a four-sided lid driven cavity are reported in the present study. The flow is generated by moving the upper wall to the right and the lower wall to the left, while moving the left wall downwards and the right wall upwards. Numerical simulations are performed by solving the unsteady two-dimensional Navier-Stokes equations in stream function-vorticity form. A compact fourth-order accurate central difference scheme is used for spatial discretization, while the second-order accurate Crank-Nicolson scheme is used for discretization of the time dependent terms. Numerical test cases show that the cavity flow remains steady up till a critical Reynolds number of 735. At this critical value, the flow undergoes a supercritical Hopf bifurcation, giving rise to a perfectly periodic state. Flow periodicity is verified through time history plots for the stream function and vorticity, Fourier power spectrum plots and phase-space trajectories. Reported streamline plots, at different time instants, clearly demonstrate the change in flow pattern during a single period and the merging and unmerging of the different vortices. Moreover, phase-space trajectories show the transition from a fixed point attractor and a steady flow regime to a limit cycle attractor and a periodic flow regime.

Keywords: driven cavity flow; bifurcation; stream function-vorticity; limit cycle; periodic flow.

1. Introduction

Lid-driven cavity flows continue to be a main topic of research in the fields of fluid mechanics and heat transfer. Although the flow geometry is comprised simply of a square, the flow dynamics inside this square are by no means simple. In fact, the driven cavity problem offers an ideal platform for the study of complex fluid flow phenomena such as vortex dynamics [1], hydrodynamic stability [2], bifurcation phenomena [3] and laminar-to-turbulent flow transition [4]. Driven cavity flow is also relevant to a number of engineering applications such as coating and drying technologies [5-7]. A detailed review of fluid dynamics in the driven cavity is given by Shankar and Deshpande [8].

^C Email: ewahba@aus.edu

Tel: +(971) 6 515 2955

Fax: +(971) 6 515 2979

© 2009-2012 All rights reserved. ISSR Journals

PII: S2180-1363(11)32100-X

Numerical simulations of steady flows in one-sided lid driven cavities were reported by numerous authors [9-12]. Accurate numerical solutions for the benchmark case of $Re=1000$ are frequently used for assessment and validation of numerical methods in the field of computational fluid dynamics. The hydrodynamic stability of the two-dimensional steady flow was also investigated in a group of studies [2, 13, 14, 15]. Beyond a critical Reynolds number, the one-sided lid driven cavity flow undergoes a supercritical Hopf bifurcation and the steady state is shown to be no longer stable. Moreover, the transition process to a chaotic flow state was numerically investigated in [4].

Recently, several studies examined the flow dynamics inside a square cavity driven by all four walls [3, 16]. In the four-sided driven cavity, the upper wall is moved to the right, the lower wall to the left, while the left wall is moved downwards and the right wall upwards, with all four walls moving with equal speeds. In such a configuration, it is shown that for low Reynolds numbers, the flow consists of four equally sized vortices, with the whole flow field being symmetric with respect to both cavity diagonals. As the Reynolds number exceeds a critical value of 129, the flow undergoes a supercritical pitchfork bifurcation and the symmetric solution is no longer stable. Instead, two stable asymmetric flow states are possible, with the initial perturbations in the flow determining which asymmetric state would be physically realized. Such an interesting flow behavior is not uncommon in fluid mechanics, with the Coanda effect and the preferential attachment of a confined jet to either one of the two confining walls, coming immediately to mind [17]. Numerical simulations performed for four-sided lid driven cavity flows covered the Reynolds number range up till a maximum value of 300 [3]. Heat transfer inside differentially heated four-sided lid driven cavities was also investigated in [18].

In the present study, numerical simulations for four sided lid driven cavity flows are extended to higher Reynolds numbers. An unsteady flow solver is used to examine the hydrodynamic stability of the flow. Hence, the study proceeds as follows. The details of the numerical procedure and the spatial and temporal discretizations are stated first. Validation of the present numerical procedure against available data in the literature for four-sided lid driven cavity flow at $Re=300$ follows. Once the numerical procedure is validated, numerical simulations for higher Reynolds numbers are performed up till a maximum value of 1000. The hydrodynamic stability of the flow will be examined through time history plots for the vorticity and stream function, phase-space trajectories and Fourier power spectrum plots.

2. Governing Equations and Numerical Methods

Consider a generic convection-diffusion equation with variable coefficients, of the form

$$\frac{\partial^2 U}{\partial x^2} + \frac{\partial^2 U}{\partial y^2} + p \frac{\partial U}{\partial x} + q \frac{\partial U}{\partial y} = f \quad (1)$$

The discretized value of the function U at a generic grid point is denoted by U_o . The discretized value at its eight neighboring points are denoted by U_i , $i=1,2,\dots,8$. Hence, the compact nine-point computational stencil is represented as follows

$$\begin{bmatrix} U_6 & U_2 & U_5 \\ U_3 & U_0 & U_1 \\ U_7 & U_4 & U_8 \end{bmatrix}$$

Similarly, the discretized values for the functions p , q and f are given as p_i , q_i and f_i $i=0,1,\dots,4$. Following [19] and for a uniform grid with spacing $\Delta x = \Delta y = h$, the compact fourth-order central difference scheme for the generic convection-diffusion equation (1) is given as

$$\sum_{i=0}^8 \alpha_i U_i = \frac{h^2}{2} [8f_0 + f_1 + f_2 + f_3 + f_4] + \frac{h^3}{4} [p_0(f_1 - f_3) + q_0(f_2 - f_4)] \tag{2}$$

where the coefficients α_i are evaluated from the following expressions

$$\alpha_0 = -[20 + h^2(p_0^2 + q_0^2) + h(p_1 - p_3) + h(q_2 - q_4)]$$

$$\alpha_1 = 4 + \frac{h}{4} [4p_0 + 3p_1 - p_3 + p_2 + p_4] + \frac{h^2}{8} [4p_0^2 + p_0(p_1 - p_3) + q_0(p_2 - p_4)]$$

$$\alpha_2 = 4 + \frac{h}{4} [4q_0 + 3q_2 - q_4 + q_1 + q_3] + \frac{h^2}{8} [4q_0^2 + p_0(q_1 - q_3) + q_0(q_2 - q_4)]$$

$$\alpha_3 = 4 - \frac{h}{4} [4p_0 - p_1 + 3p_3 + p_2 + p_4] + \frac{h^2}{8} [4p_0^2 - p_0(p_1 - p_3) - q_0(p_2 - p_4)]$$

$$\alpha_4 = 4 - \frac{h}{4} [4q_0 - q_2 + 3q_4 + q_1 + q_3] + \frac{h^2}{8} [4q_0^2 - p_0(q_1 - q_3) - q_0(q_2 - q_4)]$$

$$\alpha_5 = 1 + \frac{h}{2} (p_0 + q_0) + \frac{h}{8} (q_1 - q_3 + p_2 - p_4) + \frac{h^2}{4} p_0 q_0$$

$$\alpha_6 = 1 - \frac{h}{2} (p_0 - q_0) - \frac{h}{8} (q_1 - q_3 + p_2 - p_4) - \frac{h^2}{4} p_0 q_0$$

$$\alpha_7 = 1 - \frac{h}{2} (p_0 + q_0) + \frac{h}{8} (q_1 - q_3 + p_2 - p_4) + \frac{h^2}{4} p_0 q_0$$

$$\alpha_8 = 1 + \frac{h}{2} (p_0 - q_0) - \frac{h}{8} (q_1 - q_3 + p_2 - p_4) - \frac{h^2}{4} p_0 q_0$$

Incompressible flow in a lid driven cavity is governed by the Navier–Stokes equations. This set of nonlinear equations can be re-written in terms of a non-dimensional stream function-vorticity formulation as follows

$$\frac{\partial^2 \psi}{\partial x^2} + \frac{\partial^2 \psi}{\partial y^2} = -\omega \tag{3}$$

$$\frac{\partial \omega}{\partial t} + \mathbf{u} \frac{\partial \omega}{\partial x} + \mathbf{v} \frac{\partial \omega}{\partial y} = \frac{1}{\text{Re}} \left(\frac{\partial^2 \omega}{\partial x^2} + \frac{\partial^2 \omega}{\partial y^2} \right) \tag{4}$$

$$\mathbf{u} = \frac{\partial \psi}{\partial y}, \quad \mathbf{v} = -\frac{\partial \psi}{\partial x} \tag{5}$$

The compact fourth-order discretization (2) of the generic convection-diffusion equation (1) can be readily applied to discretize the spatial terms in the stream function equation (3) and the vorticity transport equation (4). Strictly speaking, the fourth-order discretization for the stream function equation is given by equation (2) with $U=\psi$, $p=0$, $q=0$ and $f=-\omega$. Such a discretization would result in the Mehrstellen formula [20]

$$4(\psi_1 + \psi_2 + \psi_3 + \psi_4) + \psi_5 + \psi_6 + \psi_7 + \psi_8 - 20\psi_0 = -\frac{h^2}{2} (8\omega_0 + \omega_1 + \omega_2 + \omega_3 + \omega_4)$$

On the other hand, the fourth-order discretization of the spatial terms in the vorticity transport equation is again given by equation (2) with $U=\omega$, $p=-u\text{Re}$, $q=-v\text{Re}$ and $f=0$. The temporal term is discretized using an implicit second-order accurate Crank Nicolson scheme as follows

$$\text{Re} \left(\frac{\omega_{i,j}^{n+1} - \omega_{i,j}^n}{\Delta t} \right) = \frac{1}{2} [\mathbf{R}(\omega^{n+1}) + \mathbf{R}(\omega^n)]$$

where $R(\omega)$ represents the compact fourth order discretization operator (2) applied to the spatial terms of the vorticity transport equation (4). A dual time-stepping procedure [21] is adopted where pseudo time subiterations, coupled with a line successive over-relaxation (LSOR) scheme, are used to solve the implicit set of equations at each physical time step.

A fourth-order discretization of equation (5) gives the following expressions for the velocity components, u and v , in terms of the stream function and vorticity [20]

$$u_0 = \frac{\psi_2 - \psi_4}{3h} + \frac{(\psi_5 + \psi_6 - \psi_7 - \psi_8)}{12h} + \frac{h(\omega_2 - \omega_4)}{12}$$

$$v_0 = \frac{\psi_3 - \psi_1}{3h} - \frac{(\psi_5 - \psi_6 - \psi_7 + \psi_8)}{12h} + \frac{h(\omega_3 - \omega_1)}{12}$$

The flow in the driven cavity is impulsively started with initial conditions of zero for the stream function, vorticity and velocity components u and v . To apply the no-slip boundary condition at the walls, a zero value for the stream function is enforced, while Thom's formula [22] is used as the boundary condition for vorticity.

3. Validation of Numerical Procedure

The present numerical procedure is first validated against the classical problem of a single-sided lid driven cavity. The flow domain consists of a square cavity with the upper lid being moved at a constant velocity to the left. Results for this classical flow problem are readily available in the literature for a wide range of Reynolds numbers. At $Re=5000$, a steady flow state prevails which consists of a primary vortex, two secondary vortices located in the bottom corners and a third secondary vortex in the upper right corner. Streamlines for the single-sided lid driven cavity flow at $Re=5000$, using the present numerical procedure, are given in fig (1). Moreover, table (1) provides quantitative comparisons between the present results and other results available in the literature [11, 23-25] in terms of the location of the primary vortex and the corresponding value of the stream function at the center of this vortex. The comparison shows good agreement between the present results and reported data in the literature.

The four-sided lid driven cavity is considered next. The geometry of the four-sided lid driven cavity problem is described in fig (2). The upper wall is moved to the right, the lower wall to the left, while the left wall is moved downwards and the right wall upwards, with all four walls moving with equal speeds. For low Reynolds number flows, four distinct vortices are formed; an upper vortex, a lower vortex, a right vortex and a left vortex. The resulting flow field is symmetric about both cavity diagonals [3].

As the Reynolds number is increased, symmetry with respect to the cavity diagonals is lost and the flow undergoes a supercritical pitchfork bifurcation. Two stable asymmetric flow states exist above the critical Reynolds number value of 129. In the first state, the upper and lower vortices merge to form a single primary vortex at the expense of the left and right vortices. In the second state, the primary vortex is formed through the merging of the left and right vortices [3].

For validating the numerical procedure, the $Re=300$ case is simulated in the present study on three different grids, 101×101 , 141×141 and 197×197 and compared with reported results in [3]. Comparisons between the second-order accurate values for Ψ_{GC} from [3] and present fourth-order accurate values are given in table (2) for $Re=300$. Higher-order approximations are obtained using Richardson extrapolation [12]. In fact, using the present fourth-order accurate solutions on three different grids and repeated Richardson extrapolations, one could provide numerical results that are, in theory, eighth order accurate. Such extrapolated values are reported in table (2) for the $Re=300$ case.

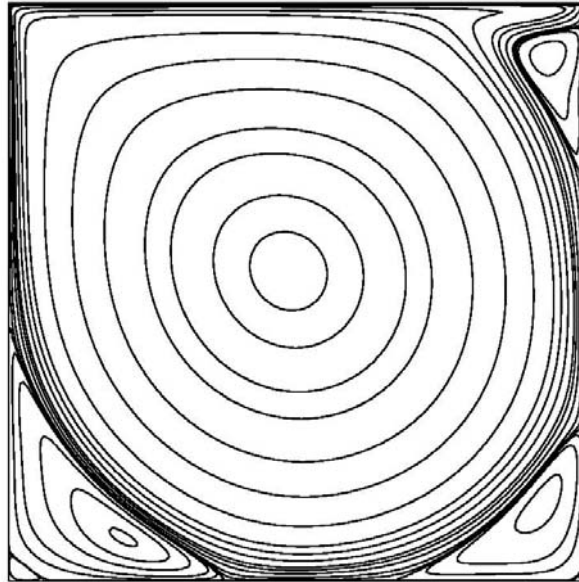


Figure 1. Streamlines for single-sided lid driven cavity flow (Re=5000)

TABLE1: PRIMARY VORTEX PROPERTIES FOR SINGLE-SIDED LID DRIVEN CAVITY FLOW (RE=5000)

Reference	Grid	ψ	x	y
Present	197 x 197	0.1202	0.48469	0.53571
Ghia et al [11]	256 x 256	0.118966	0.4883	0.5352
Bruneau & Saad [23]	256 x 256	0.12064	0.48438	0.53516
Bruneau & Saad [23]	2048 x 2048	0.12197	0.48535	0.53516
Goodrich [24]	256 x 256	0.118	0.48438	0.53516
Pan & Glowinski [25]	256 x 256	0.121218	0.4844	0.5352

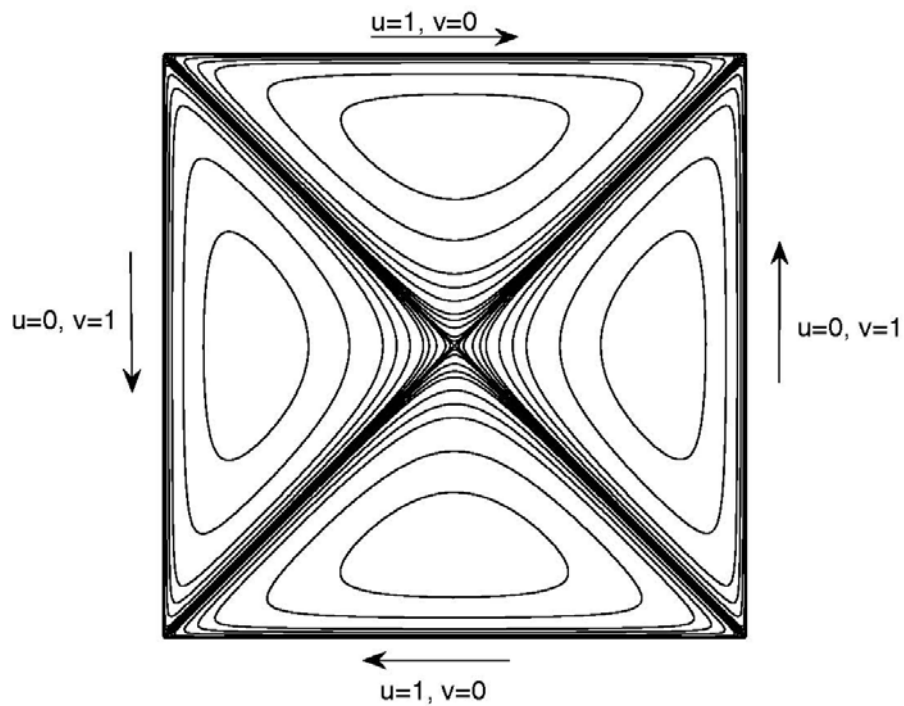


Figure 2. Geometry of the four-sided lid driven cavity problem

TABLE2: Ψ_{GC} VALUES FOR FOUR-SIDED LID DRIVEN CAVITY FLOW (RE=300)

Study	Grid	Order of accuracy	Value of Ψ_{GC}
Wahba [3]	100x100	Δh^2	$\Psi_{GC} = -0.1106$
Wahba [3]	150x150	Δh^2	$\Psi_{GC} = -0.1121$
Wahba [3]	200x200	Δh^2	$\Psi_{GC} = -0.1127$
Present	101x101	Δh^4	$\Psi_{GC} = -0.11326$
Present	141x141	Δh^4	$\Psi_{GC} = -0.11334$
Present	197x197	Δh^4	$\Psi_{GC} = -0.11336$
Present	Extrapolated	Δh^8	$\Psi_{GC} = -0.11337$

4. Steady flow regime

Previous work on four-sided lid driven cavity flow considered Reynolds number values up till 300. In the present study, the time-dependent numerical procedure, discussed in section II, is used to extend the four-sided lid driven cavity flow to higher Reynolds numbers. Specifically, numerical simulations are performed for two different Reynolds numbers; 710 and 740. A 141x141 grid is used in both simulations. Results of the simulations are given in figs (3) and (4) for Re=710 and Re=740 respectively. Time histories for the stream function and vorticity at the cavity center show the Re=710 case converging to a steady state. On the other hand, the corresponding plots for Re=740 indicate a periodic flow behavior.

Moreover in fig (5), phase space-trajectories clearly show the transition from a fixed point attractor and a steady flow regime in the Re=710 case to a limit cycle attractor and a periodic flow regime in the Re=740 case. Fourier power spectrum plot for Re=740 reveals a fundamental frequency value of 0.09, as shown in fig (6).

The above numerical test cases show that the flow inside the cavity remains steady up till a critical Reynolds number, Re_{cr} . At this critical value, the flow undergoes a supercritical Hopf bifurcation which gives rise to a perfectly periodic state. In order to determine the value of Re_{cr} , steady and periodic flows on either side of the bifurcation point are computed yielding an ever-decreasing range of Reynolds numbers in which the bifurcation must occur. Two different grids are used for the evaluation of Re_{cr} ; 101x101 and 141x141. Numerical simulations using the 101x101 grid predict $Re_{cr}=715\pm 4$, while simulations using the 141x141 grid predict $Re_{cr}=735\pm 4$.

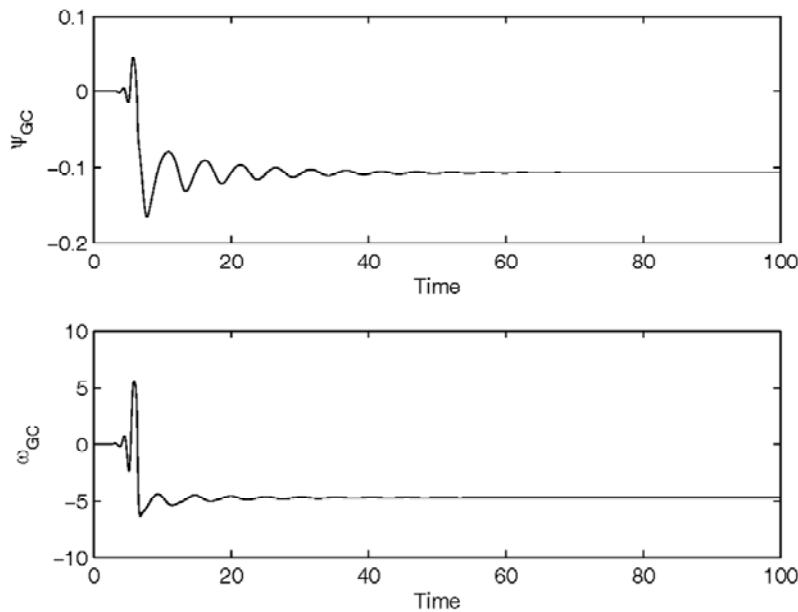


Figure 3. Time histories for stream function and vorticity at the cavity center (Re=710)

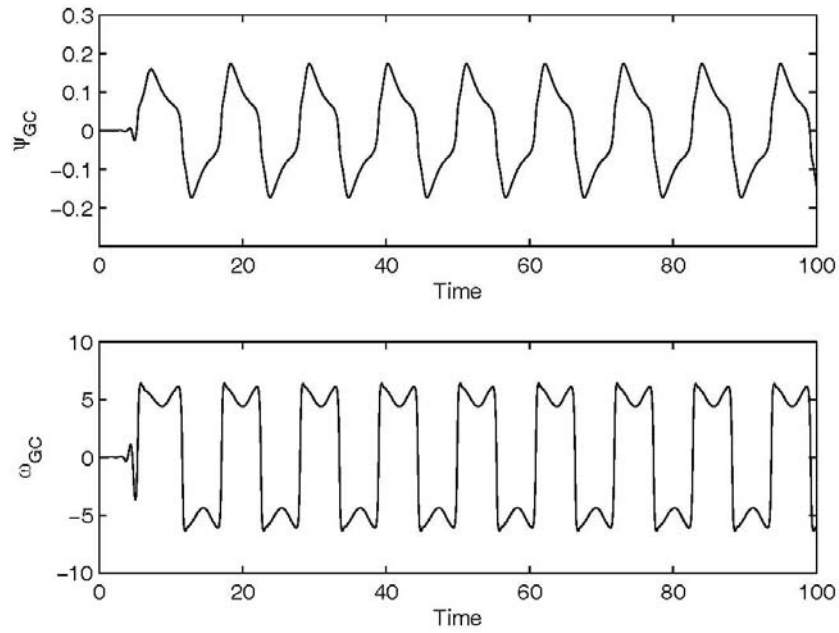


Figure 4. Time histories for stream function and vorticity at the cavity center (Re=740)

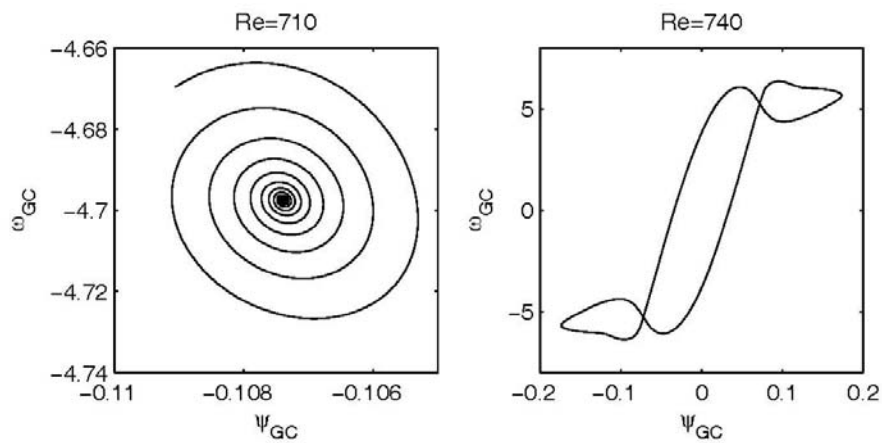


Figure 5. Phase-space trajectory (Re=710 & Re=740)

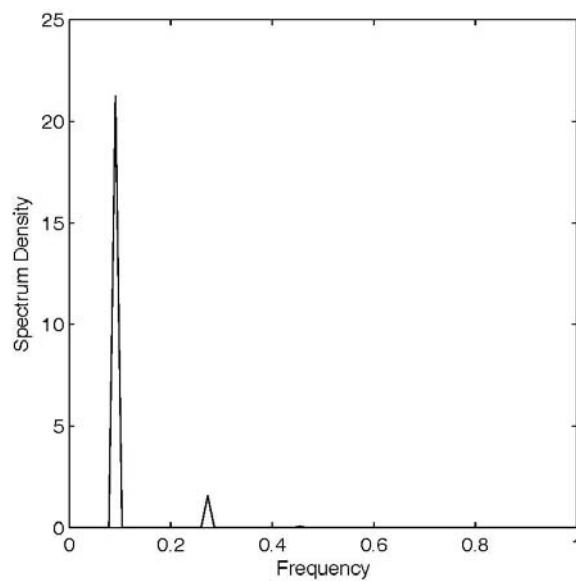


Figure 6. Fourier power spectrum for Re=740

5. Periodic flow regime

Numerical results for $Re=1000$ are given in fig (7) in terms of time histories of stream function and vorticity at the cavity center, Fourier power spectrum plots and phase-space trajectories. The figures verify the periodic nature of the flow with a fundamental frequency of 0.142. The phase-space trajectory is shown to no longer converge to a fixed point attractor, but rather to a limit cycle attractor, indicating a periodic flow state.

Moreover, for $Re=1000$, streamline plots at different time instants during a single period are reported in fig (8). The plots show the drastic temporal changes in the flow patterns and the merging and unmerging of the different vortices. At the beginning of the period ($t=0.0T$), the upper and lower vortices are merged together into a single primary vortex, at the expense of the right and left vortices. As time advances ($t=0.125T, 0.25T$), the left and right vortices grow in size while the primary vortex shrinks. At ($t=0.375T$), the primary vortex splits back into two upper and lower vortices, with the left and right vortices now merging to form the new primary vortex. As time again advances ($t=0.5T, 0.625T$ and $0.75T$), the size of the primary vortex increases till it reaches a maximum then decreases. At time ($t=0.875T$), the primary vortex splits back into two right and left vortices, with the upper and lower vortices merging to form a new primary vortex. The size of this primary vortex starts to grow with time such that at ($t=T$), it reaches the exact size it had at ($t=0.0T$) and a single cycle is completed.

To further assess grid independence of the time-dependent results, the phase-space trajectory for $Re=1000$ is given in fig (9) using two different grids; 101×101 and 141×141 . Fig (9) reveals good agreement between the limit cycle attractors predicted by both grids. Moreover, the fundamental frequency for the periodic flow predicted by both grids match very closely, with the 101×101 grid giving a frequency of 0.141 as compared to a frequency of 0.142 on the 141×141 grid.

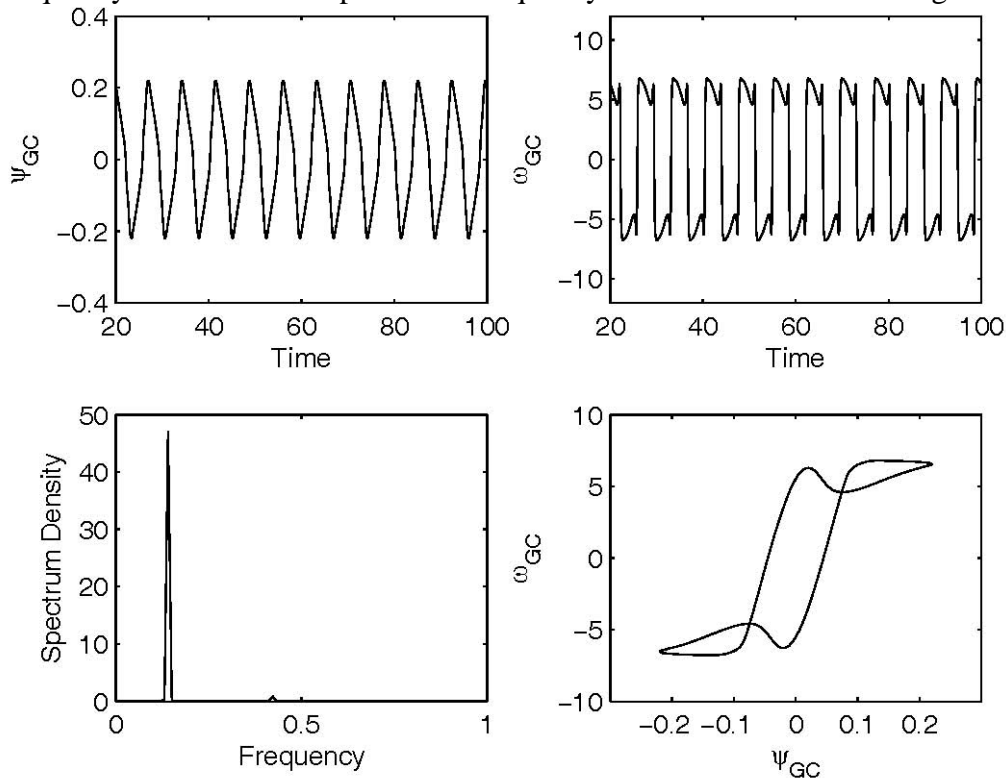


Figure 7. Time histories, phase-space and power spectrum plots for $Re=1000$

6. Concluding Remarks

Four-sided lid driven cavity flows are shown to undergo a supercritical Hopf bifurcation at a critical Reynolds number of 735 ± 4 . Below this critical value, the flow inside the cavity is steady with

a fixed point attractor. Above this critical value, the flow becomes periodic with a limit cycle attractor. Grid independence is verified through numerical simulations on three different grids for the steady flow regime, and two different grids for the periodic flow regime. Using simulations on three grids in the steady flow regime and repeated Richardson extrapolations, numerical results of eighth order accuracy are presented for the $Re=300$ case. On the other hand, for Reynolds numbers larger than Re_{cr} , periodicity of the flow is verified through time history plots, phase space-trajectories and power spectrum plots. The periodic flow regime is realized up till a Reynolds number of 1000, which is the maximum Reynolds number value considered in the present study.

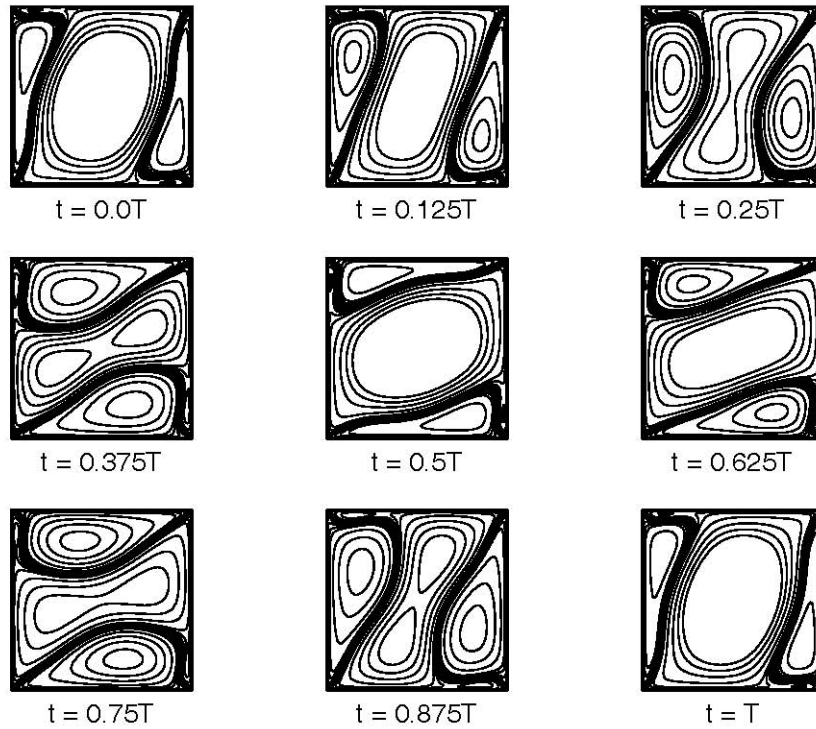


Figure 8. Time evolution of the streamlines during one complete cycle for $Re=1000$

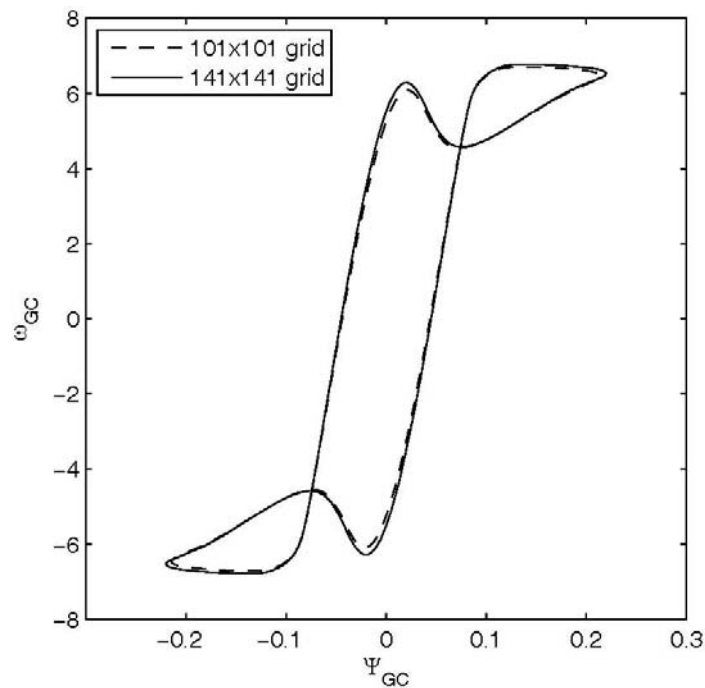


Figure 9. Phase-space trajectory computed on two different grids for $Re=1000$

Nomenclature

L:	Length of square cavity side
t:	Time
u:	Horizontal component of velocity
v:	Vertical component of velocity
V:	Velocity of the driven cavity side
x:	Horizontal location
y:	Vertical location
ν :	Kinematic viscosity
ψ :	Stream function
ψ_{GC} :	Stream function at the geometric center of the square cavity
ω :	Vorticity
ω_{GC} :	Vorticity at the geometric center of the square cavity
Re:	Reynolds number = VL/ν
Re _{cr} :	Critical Reynolds number for Hopf bifurcation

References

- [1] Cheng M, Hung KC, Vortex structure of steady flow in a rectangular cavity, *Computers & Fluids*, 2006. 35: p. 1046–62.
- [2] Bruneau Ch-H, Saad M, The 2D lid-driven cavity problem revisited, *Computers & Fluids*, 2006. 35: p. 326–48.
- [3] Wahba, EM, Multiplicity of states for two sided and four sided lid driven cavity flows, *Computers & Fluids*, 2009. 38: p. 247–53.
- [4] Peng YF, Shiau YH, Hwang RR., Transition in a 2-D lid-driven cavity flow, *Computers & Fluids*, 2003. 32: p. 337–52.
- [5] Aidun C.K, Triantafillopoulos NG, Benson JD., Global stability of a lid-driven cavity with through flow: flow visualization studies, *Physics of Fluids*, 1991. 3: p. 2081–91.
- [6] Alleborn N, Raszillier H, Durst F., Lid-driven cavity with heat and mass transport, *International Journal of Heat Mass Transfer*, 1999. 42: p. 833–53.
- [7] Zdanski PSB, Ortega MA, Fico Jr Nide GCR., Numerical study of the flow over shallow cavities, *Computers & Fluids*, 2003. 32: p. 953–74.
- [8] Shankar PN, Deshpande MD., Fluid mechanics in the driven cavity, *Annual Review of Fluid Mechanics*, 2000. 32: p.93–136.
- [9] Burggraf OR., Analytical and numerical studies of the structure of steady separated flows, *Journal of Fluid Mechanics*, 1966. 24: p. 113–5.
- [10] Pan F. and Acrivos, A., Steady flows in rectangular cavities, *Journal of Fluid Mechanics*, 1967. 28: p. 643–655.
- [11] Ghia U, Ghia KN, Shin CT., High-Re solutions for incompressible flow using the Navier–Stokes equations and a multigrid method, *Journal of Computational Physics*, 1982. 48: p. 387–411.
- [12] Schreiber R, Keller HB, Driven cavity flows by efficient numerical techniques, *Journal of Computational Physics*, 1983. 49: p. 310–33.
- [13] Poliashenko M and Aidun CK, A direct method for computation of simple bifurcations. *Journal of Computational Physics*, 1995. 121: p. 246–60.
- [14] Nobile E, Simulation of the time-dependent flow in cavities with the additive-correction multigrid method. Part II: Applications, *Numerical Heat Transfer, Part B*, 1996. 30: p. 351–70
- [15] Auteri F, Parolini N and Quartapelle L, Numerical investigation on the stability of singular driven cavity flow, *Journal of Computational Physics*, 2002. 183: p. 1–25.
- [16] Perumal DA and Dass AK, Multiplicity of steady solutions in two-dimensional lid-driven

cavity flows by Lattice Boltzmann Method, *Computers & Mathematics with Applications*, in press, [doi:10.1016/j.camwa.2010.03.053](https://doi.org/10.1016/j.camwa.2010.03.053)

- [17] Wahba EM, Iterative solvers and inflow boundary conditions for plane sudden expansion flows, *Applied Mathematical Modelling*, 2007. 31: p. 2553-2563.
- [18] Wahba EM and Gadalla MA, Heat and fluid flow characteristics inside differentially heated square enclosures with single and multiple sliding walls, *Heat Transfer - Asian Research*, 2009. 38: p. 422-34.
- [19] Gupta MM, Manohax RP and Stephenson JW, A single cell high order scheme for the convection-diffusion equation with variable coefficients, *International Journal for Numerical Methods in Fluids*, 1984. 4: p. 641-51.
- [20] Gupta MM, A fourth-order Poisson solver, *Journal of Computational Physics*, 1984. 55: p.166-72.
- [21] Rogers SE and Kwak D, Upwind differencing scheme for the time-accurate incompressible Navier–Stokes equations, *AIAA Journal*, 1990. 28: p. 253–62.
- [22] Thom A, The Flow Past Circular Cylinders at Low Speed, *Proc. Roy. Soc. Lond. A.*, Vol. 141, 1933, pp. 651–669.
- [23] Bruneau Ch-H, Saad M, The 2D lid-driven cavity problem revisited, *Computers and Fluids*, 2006. 35: p. 326–48.
- [24] Goodrich U, An unsteady time-asymptotic flow in the square driven cavity, *IMACS 1st International Conference on Computational Physics*, Boulder; 1990
- [25] Pan T.W. and Glowinski R., A projection/wave-like equation method for the numerical simulation of incompressible viscous fluid flow modeled by the Navier–Stokes equations, *Computational Fluid Dynamics Journal*, 2000. 9: p. 28-42.